Journal of CO2 Utilization 108 (2026) 103426

Contents lists available at ScienceDirect

Journal of CO2 Utilization

journal homepage: www.elsevier.com/locate/jcou

Single-amine strategy for CO_2 hydrogenation to formic acid: Process simplification using NBIM coupled with heterogeneous Ru-MACHO-POMP catalysis

Jiseong Baek [a,1], Jaehyeong Choi [b,c,1], Hongjin Park [a,1], Minsol Kim [b,c], Ki Bong Lee [c], Ung Lee [b,d,e,*], Sungho Yoon [a,**]

[a] Department of Chemistry, Chung-Ang University, Seoul 06974, Republic of Korea
[b] Clean Energy Research Center, Korea Institute of Science and Technology (KIST), Hwarang-ro 14-gil 5, Seongbuk-gu, Seoul 02792, Republic of Korea
[c] Department of Chemical and Biological Engineering, Korea University, Anam-ro 145, Seongbuk-gu, Seoul 02841, Republic of Korea
[d] Division of Energy and Environmental Technology, KIST School, Korea University of Science and Technology (UST), Seoul 02792, Republic of Korea
[e] Graduate School of Energy and Environment (Green School), Korea University, Seoul 02841, Republic of Korea

ARTICLE INFO

Keywords:
CO_2 hydrogenation
Formic acid production
Single-amine system
Heterogeneous catalysis
TEA-LCA analysis

ABSTRACT

The catalytic hydrogenation of carbon dioxide (CO_2) to formic acid (FA) is a promising pathway for sustainable C1 chemical production and hydrogen storage; however, practical implementation is often limited by complex separation processes associated with conventional dual-amine systems. Herein, we propose a simplified single-amine strategy in which N-butylimidazole (NBIM) functions simultaneously as both the reaction and separation amine, eliminating the amine-exchange step and reducing process complexity. To compensate for the relatively low basicity of NBIM, heterogeneous catalysts were systematically screened, and a porous polymer–immobilized Ru-MACHO catalyst (Ru-MACHO-POMP) exhibited the highest activity under NBIM-based conditions, achieving a formate productivity of 53 $kg_{FA}/kg_{cat.}$/d. at 80 °C and 80 bar. Temperature-dependent studies revealed that operation at moderate temperature enables a favorable balance between reaction productivity and acid-to-amine ratio (AAR), which is a critical parameter governing downstream separation energy. Based on the optimized reaction conditions, process simulation and techno-economic analysis (TEA) were conducted, demonstrating a levelized cost of FA of \$0.583 kg^{-1} , comparable to conventional fossil-based production routes. This work demonstrates that integrating catalyst design with process simplification enables a viable pathway toward economically competitive CO_2-to-formic acid production using a single-amine platform.

1. Introduction

Catalytic conversion of carbon dioxide (CO_2) into value-added chemicals has attracted considerable attention as a key strategy to address climate change and to realize a sustainable chemical industry; CO_2 is regarded as a versatile C_1 feedstock that can be transformed into fuels and commodity chemicals, including methanol, methane, urea, and formic acid (HCO_2H) [1–4]. Among these products, formic acid is an industrially relevant chemical used in agricultural and leather applications and has also emerged as a promising hydrogen storage and transportation medium owing to its low toxicity and high thermal stability [5,6]. Notably, formic acid possesses a high volumetric hydrogen density of approximately 53 g L^{-1}, which significantly exceeds that of compressed gaseous hydrogen at 200 bar (ca. 16 g L^{-1}) [7,8].

However, most formic acid produced industrially at present relies on fossil-resource-based processes, such as methanol carbonylation followed by hydrolysis [9]. These routes require high-purity carbon monoxide, leading to high production costs and an inherent inability to avoid net CO_2 emissions throughout the process [10]. To address these limitations, the direct thermocatalytic hydrogenation of CO_2 to formic acid has emerged as a more sustainable and potentially carbon-neutral alternative [11].

* Corresponding author at: Clean Energy Research Center, Korea Institute of Science and Technology (KIST), Hwarang-ro 14-gil 5, Seongbuk-gu, Seoul 02792, Republic of Korea.
** Corresponding author.
E-mail addresses: ulee@kist.re.kr (U. Lee), sunghoyoon@cau.ac.kr (S. Yoon).
[1] These authors contributed equally to this work.

https://doi.org/10.1016/j.jcou.2026.103426
Received 25 February 2026; Received in revised form 12 March 2026; Accepted 12 April 2026
Available online 28 April 2026
2212-9820/© 2026 The Authors. Published by Elsevier Ltd. This is an open access article under the CC BY license (http://creativecommons.org/licenses/by/4.0/).

In CO_2 hydrogenation, the direct accumulation of free formic acid (FA) is thermodynamically highly unfavorable under neutral conditions, as reflected by the small equilibrium constant of the reaction (Eq. 1) [12]. To overcome this limitation, a common strategy is to employ a basic aqueous medium, in which the generated formic acid is stabilized as the formate anion (Eqs. 2 and 3) [13,14].

$$CO_2(g) + H_2(g) \rightleftharpoons HCOOH(l)\ \Delta G^{\circ}_{298} = 32.9 kJmol^{-1} \quad (1)$$

$$CO_2(g) + H_2(g) + NH_3(aq) \rightleftharpoons NH_4^+(aq) + HCOO^-(aq)\ \Delta G^{\circ}_{298} = -9.5 kJmol^{-1} \quad (2)$$

$$CO_2(aq) + H_2(aq) + NH_3(aq) \rightleftharpoons NH_4^+(aq) + HCOO^-(aq)\ \Delta G^{\circ}_{298} = -35.4 kJmol^{-1} \quad (3)$$

In industrial processes, amine-based bases are commonly used because they can be recovered and regenerated after the reaction. However, when primary or secondary amines are employed, they tend to undergo condensation with formic acid to formamides, which complicates separation and regeneration by distillation [15,16]. Tertiary amines, which can be efficiently regenerated via distillation, have been predominantly preferred in practical CO_2 hydrogenation–to–formic acid processes [17,18].

Triethylamine, which has been widely employed as a tertiary amine base in CO_2 hydrogenation–to–formic acid processes, forms an azeotrope with formic acid at an approximate molar ratio of 2.3:1 [19]. As a result, the separation step requires high-temperature and high-vacuum conditions, which in turn raise concerns regarding the thermal decomposition of formic acid [20–22]. To address this separation challenge, several approaches have been proposed. Barbera *et al.* introduced a pretreatment step based on an adiabatic gas–liquid–liquid flash separator, Mahida proposed pressure-swing distillation, and Ci *et al.* developed a fixed-bed continuous-flow system; however, these strategies generally involve complex separation units and high energy consumption, ultimately leading to increased capital and operating costs [23–25].

As an alternative to these limitations, the dual amine system has been developed. In this approach, triethylamine, which has a relatively high pK_a, is initially employed to secure sufficient reactivity during CO_2 hydrogenation, after which amine exchange is induced with an auxiliary amine possessing a lower pK_a and a higher boiling point (e.g., imidazole derivatives) to improve the efficiency of formic acid separation [26,27]. To further extend this concept, Kim *et al.* developed a dual-amine process using N-methylpiperidine (NMPI), introduced as an alternative to triethylamine, as the reaction amine and N-butylimidazole (NBIM) as the separation amine, and demonstrated its feasibility at the pilot scale (~10 kg·day^{-1}) (Fig. 1a). Nevertheless, the additional energy consumption, thermal load, and the requirement for dedicated columns associated with the amine exchange step remain factors that adversely affect the overall process economics [28,29].

In this study, we propose a strategy to improve the economic viability of the dual-amine process by addressing its inherent complexity. Specifically, we introduce an imidazole derivative as a single amine that simultaneously serves as both the reaction amine and the separation amine, thereby eliminating the amine-exchange step (Fig. 1b). NBIM was selected as the sole amine owing to its physicochemical properties that are favorable for formic acid recovery via distillation-based separation. Although NBIM exhibits a lower pK_a than conventional tertiary amines, which can lead to reduced reaction rates, the performance of the NBIM-based single-amine process was systematically evaluated through a comparative assessment of previously reported heterogeneous catalysts. Furthermore, life-cycle assessment (LCA) and techno-economic analysis (TEA) were conducted to quantitatively compare the changes in energy consumption, cost, and environmental impact resulting from process simplification, thereby discussing the industrial applicability of the NBIM single-amine process.

2. Results and discussion

2.1. Design of the single-amine system

Because a single amine must simultaneously enable CO_2 hydrogenation and distillation-based formic acid (FA) recovery, it should exhibit low volatility, limited acid–base association with FA, and preferably form an azeotrope at a low FA mole fraction, thereby improving separability toward high-purity FA.

NBIM exhibits a high boiling point of 280 °C and a low vapor pressure at ambient conditions, which minimizes volatilization losses during distillation-based separation [30]. In addition, its pK_a (≈ 7.09) is lower than that of typical tertiary amines, resulting in relatively weaker ion-pair interactions with FA. Moreover, the FA–NBIM system has been reported to form an azeotrope with a FA mole fraction of around 0.30, providing favorable separation characteristics from the perspective of high-purity FA recovery [29].

However, the relatively low pK_a of imidazole-based amines including NBIM weakens the thermodynamic driving force for CO_2 hydrogenation and can lead to reduced reaction rates. Indeed, de Leeuw den Bouter *et al.* reported that, in the CO_2 hydrogenation of aqueous NBIM over an

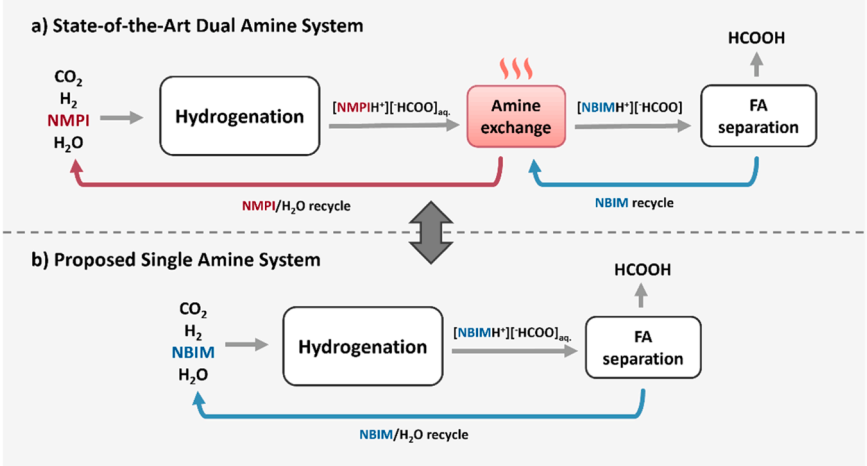


Fig. 1. Schematic diagram for thermocatalytic CO_2 hydrogenation to FA. (a) Dual-amine process employing NMPI as the reaction amine and NBIM as the separation amine, as reported by Kim *et al.* (b) New single-amine process proposed in this work, in which NBIM serves as both reaction and separation amine, eliminating the amine-exchange step.

Au/TiO_2 catalyst, the initial rate of formic acid formation was lower than that observed under otherwise identical conditions using a tertiary amine [20]. Therefore, to simplify the process by employing NBIM as both the reaction and separation amine, the development of a highly active catalyst capable of compensating for the reduced reactivity associated with the low pK_a environment is essential. In summary, the design concept of this study is to directly translate the favorable physicochemical properties of NBIM that enable facile FA separation into process simplification, while addressing the key kinetic bottleneck through catalyst design.

A wide range of catalytic systems have been reported for the production of FA via CO_2 hydrogenation, providing an important background for catalyst selection in this study. CO_2 hydrogenation is highly catalyst-dependent, and achieving practical reaction rates requires catalysts with high intrinsic activity. Homogeneous metal catalysts generally exhibit excellent catalytic performance, including high product selectivity, and in some cases have achieved high reaction rate even under mild reaction conditions [31,32]. Despite their superior reactivity, however, homogeneous catalysts suffer from practical limitations, as contact between the catalyst and FA during downstream purification can lead to FA decomposition, necessitating additional catalyst separation and recovery steps. These requirements ultimately impose constraints on process robustness and operational stability [33].

In contrast, heterogeneous catalysts offer significant advantages from a process perspective owing to their facile separation after reaction, and are therefore considered a promising alternative for ensuring stable separation and purification of FA [12,34]. However, most previously reported heterogeneous catalysts suffer from relatively low catalytic activity and product selectivity, often requiring harsh reaction conditions such as elevated temperatures and pressures. For example, a $RuCl_3@TN_{20}Bpy_1$-CTF achieved a productivity of about 600 $g_{FA}/g_{cat.}/d$ in CO_2 hydrogenation at 120 °C; but, activity dropped significantly under lower-temperature conditions, which limited its practical use [28].

Substantial efforts have been devoted to improving the conversion efficiency and selectivity of heterogeneous catalysts, especially through the design of highly active catalysts based on phosphine ligands. Immobilized macroligand-based Ru–phosphine catalysts initially displayed high CO_2 conversion [35]; however, gradual deactivation has been observed during reaction due to the formation of Ru–carbonyl species and oxidative degradation of the phosphine ligands. More recently, catalysts introduced phosphine ligands into porous polymer frameworks via a facile Friedel–Crafts-type hypercross-linking strategy. These systems are promising heterogeneous catalysts, as they give a favorable balance between high catalytic activity and improved process stability [36].

Based on this background, we focused on a Ru-MACHO-based catalyst that was previously reported by our group, in which the homogeneous Ru-MACHO complex is immobilized within a porous organometallic polymer (POMP) framework (Ru-MACHO-POMP) [37]. This catalyst has demonstrated high catalytic activity and product selectivity across a range of hydrogenation reactions, and has been shown to retain excellent activity even under low-temperature conditions. Accordingly, Ru-MACHO-POMP was identified as a promising catalyst candidate for operation under NBIM conditions, and its performance was comparatively evaluated alongside other hydrogenation catalysts within the NBIM-based system.

The heterogeneous Ru-MACHO-POMP catalyst used in this study was synthesized following a previously reported Friedel–Crafts-type alkylation strategy. In the presence of $AlCl_3$, the aromatic moieties of the PNP ligand in Ru-MACHO were cross-linked via $–CH_2–$ bridges to form an insoluble porous organometallic polymer network, thereby immobilizing the Ru–PNP active sites within the polymeric framework.

The morphological and structural characteristics were consistent with those reported previously. FE-SEM/EDS analyses revealed that Ru was uniformly distributed within aggregated particles on the micrometer scale (Fig. S2). X-ray photoelectron spectroscopy and solid-state ^{13}C CP/MAS NMR analyses confirmed preservation of the Ru(II) oxidation state and the $–CH_2–$-bridged aromatic framework, respectively. Powder X-ray diffraction patterns and N_2 adsorption–desorption measurements indicated an amorphous microporous structure, with a BET specific surface area of approximately 560 $m^2\ g^{-1}$. In addition, ICP–OES analysis determined a Ru loading of 10.4 wt%.

2.2. Catalytic activity assessment

To identify a suitable heterogeneous catalyst for our proposed NBIM-based single-amine system, four different CO_2 hydrogenation catalysts were comparatively evaluated under identical reaction conditions (Fig. 2, Table 1). Catalytic performance was evaluated at 80 °C and 80 bar ($H_2/CO_2 = 1:1$) using a 1.0 M aqueous NBIM solution with 10 mg of catalyst for a reaction time of 1 h. The catalyst set was selected to represent three different active-site design strategies: (i) a commercial metal nanoparticle catalyst (Pd/C), (ii) Ru precursor immobilization on porous supports ($RuCl_3@TN_{20}Bpy_1$-CTF and $RuCl_3$@PP-POP), (iii) direct incorporation of a preorganized Ru–PNP organometallic complex into a porous polymer framework (Ru-MACHO-POMP). The commercial Pd/C catalyst was used as received, and the other catalysts were synthesized according to previously reported procedures [28,38].

All experiments were run in a batch reactor, and details are described in the Experimental Section (Fig. S1). During the reaction, reactor pressure decreased gradually, indicating the consumption of gaseous components as CO_2 hydrogenation proceeded. After the reaction time, the reactor was cooled to room temperature and vented. The catalyst settled at the bottom of the reactor after the reaction, allowing easy separation between the solid catalyst and the reaction solution. Indeed, the solid catalyst was readily recovered from the post-reaction mixture by simple filtration.

In this study, product quantification was carried out using HPLC techniques. It has been reported that formic acid–based samples can undergo thermal and/or catalytic decomposition during GC analysis [39]. The performance metrics for each catalyst are comprehensively summarized in Table 1.

Because the NBIM-based single-amine medium imposes a lower-basicity environment than conventional tertiary amine systems, catalyst performance is expected to depend strongly on intrinsic H_2-activation ability and the stability of the molecularly defined Ru active site. As summarized in Table 1, $RuCl_3@TN_{20}Bpy_1$-CTF was found to exhibit a pronounced amine-dependent reactivity. In a triethylamine-based continuous process, a formate productivity of 51.7 $g_{formate}/g_{cat.}/d$ was reported at 80 °C, whereas under NBIM-based conditions no detectable formate was formed at the same temperature (80 °C), indicating an essentially inactive behavior [28]. For Pd/C, Park *et al.* reported an average formate productivity of 420 $mmol_{FA}/g_{Pd,surf}/h$ at 80 °C in a trickle-bed continuous reactor [40]. However, the productivity gradually declined during continuous operation (e.g., ~20% loss after 20 h at 120 °C), which was attributed to catalyst deactivation via Pd nanoparticle sintering and Pd leaching. Gunasekar *et al.* further demonstrated that a bisphosphine-based porous organic polymer immobilizing Ru ($RuCl_3$@PP-POP) enables CO_2 hydrogenation to DMF, showing a measurable activity even at 80 °C and 2 MPa (combined FA+DMF yield of 10%, TON = 5000) [41]. The performance improved with increasing temperature, reaching 36% yield (TON = 18,250) at 140 °C, and the authors provided evidence for suppressed Ru leaching and good recyclability based on filtration/ICP analyses and reuse tests.

These precedents suggest that even catalysts active in conventional tertiary/secondary amine media can show lower reactivity or become kinetically constrained in single-amine environments such as NBIM. Nonetheless, in the present study, Ru-MACHO-POMP produced a formate productivity of 53 $kg_{FA}/kg_{cat.}/d$. under NBIM-based CO_2-to-formate conditions, the highest among the catalysts tested. While achieving high activity in NBIM single-amine systems is intrinsically

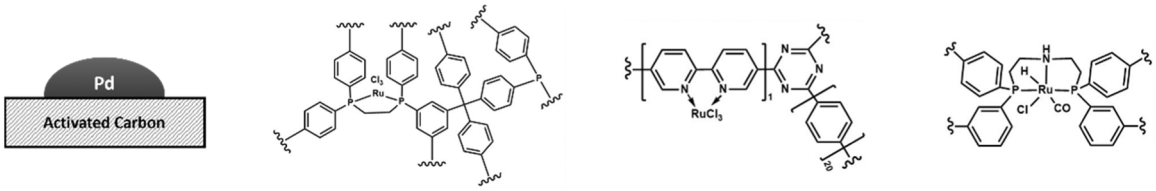


Fig. 2. Heterogeneous catalysts screened for CO_2 hydrogenation to FA in the NBIM system.

Table 1
Catalytic performance of heterogeneous catalysts for CO_2 hydrogenation to formate in the NBIM system.

Entry	Catalysts	Concentration of generated formate (M)	Productivity (kg_{FA}/$kg_{cat.}$/d.)
1	$RuCl_3$@$TN_{20}Bpy_1$-CTF	0.000	0
2	Pd@C	0.004	8
3	$RuCl_3$@PP-POP	0.013	28
4	Ru-MACHO-POMP	0.024	53

[a]Reaction condition: catalyst (10 mg), 1 M NBIM (H_2O (17.41 g, 17.41 mL) + NBIM (2.48 g, 2.59 mL)), 80 °C, 80 bar (H_2:CO_2 = 1:1) for 1 h.

more challenging than in conventional amine media, Ru-MACHO-POMP remains a promising catalyst candidate capable of providing practically meaningful productivities.

The high productivity of Ru-MACHO-POMP observed under NBIM-based conditions comes from its high intrinsic activity of the catalyst. In Ru-catalyzed CO_2 hydrogenation, H_2 first coordinates to the active site and undergoes heterolytic cleavage to form a metal hydride (Ru–H), a step that has been reported to operate as the rate-determining step [42,43]. Accordingly, catalysts that can efficiently activate H_2 and rapidly generate Ru–H species are better able to mitigate the kinetic penalty imposed under these conditions (Fig. S3).

The PNP (pincer) motif of homogeneous Ru-MACHO plays a critical role in its high intrinsic activity. The strong σ-donating phosphine groups electronically stabilize the Ru center, enabling enough hydricity needed for effective hydride transfer, while the rigid pincer framework and chelating coordination stabilize the catalytically active species during reaction, thereby favoring sustained turnover [44]. Furthermore, the bifunctional metal–ligand cooperation (MLC) characteristic proposed for Ru-MACHO systems facilitates the heterolytic cleavage of H_2 and the formation of Ru–H species, which can efficiently deliver hydride to CO_2, producing formate through a favorable pathway [45,46].

Heterogeneous Ru-MACHO-POMP has been reported to retain approximately 90% of the activity of its homogeneous Ru-MACHO counterpart under identical conditions [37]. Ru-MACHO-POMP delivered the highest productivity under NBIM-based conditions, offering clear process advantages by enabling a reduction in catalyst loading and reactor size for a given production rate. These results indicate that, under the kinetically demanding NBIM single-amine environment, merely immobilizing Ru precursors on porous supports is insufficient; instead, a catalyst platform incorporating a preorganized Ru–PNP active site with high intrinsic hydrogenation activity is required. On this basis, Ru-MACHO-POMP was selected as the benchmark catalyst for subsequent reaction and process studies.

Reaction conditions: Ru-MACHO-POMP (50 mg), 1.0 M NBIM aqueous solution (H_2O 17.41 mL; NBIM 2.59 mL), 80 bar total pressure (H_2/CO_2 = 1:1).

In thermocatalytic CO_2 hydrogenation to formic acid, the attainable product concentration is determined by both catalytic activity and liquid-phase reaction equilibrium. Accordingly, formate formation in this system showed equilibrium-limited behavior, approaching a plateau beyond a certain concentration. The maximum attainable conversion is governed by the stability limit of the FA–amine adduct that can be accommodated in the solution. To quantitatively verify this behavior, the amount of formate formed over time was monitored at different temperatures. (Fig. 3a, Table. S1). At 60, 80, 100, and 120 °C, the FA concentrations formed within the initial 1 h were 0.026, 0.09, 0.31, and 0.54 M, respectively, indicating that the initial formation rate increases with increasing temperature. In contrast, upon extended operation (144 h), the system approached a quasi-equilibrium state, and the final FA concentrations decreased markedly with increasing temperature, reaching 1.05 M at 60 °C, 0.91 M at 80 °C, 0.75 M at 100 °C, and 0.57 M at 120 °C.

In a single-amine process, formic acid must be directly purified from the post-reaction solution, rendering the acid-to-amine ratio (AAR) a critical design parameter that governs the energy demand of the downstream separation section; AAR is defined as the molar concentration of generated formic acid relative to that of the amine introduced into the reaction system ([FA]/[amine]$_0$). AAR can thus be regarded as a process parameter representing the maximum achievable conversion. At a given FA production rate, a higher AAR corresponds to a higher fraction of FA in the reaction solution, thereby reducing the circulation load of water and amine that must be removed in the purification column and consequently lowering the reboiler duty and overall utility consumption. In conventional dual amine processes, strategies have been proposed in which water and amine are selectively removed via an evaporator downstream of the reactor to increase the AAR prior to amine exchange and FA purification [29]. By contrast, because the single-amine system intrinsically couples reaction and separation around the same amine, achieving a high AAR at the reaction stage itself represents the most direct means of reducing the separation burden.

In this context, operating at low temperature becomes an important strategy for increasing the AAR in a single-amine process. Formate formation via CO_2 hydrogenation is an exothermic equilibrium reaction, and because gaseous CO_2 and H_2 are converted into ionic or adduct species in the liquid phase (e.g., formate species), the product-side equilibrium is generally favored under high-pressure and low-temperature conditions [47]. This trend indicates that increasing temperature thermodynamically favors the decomposition of FA–amine adducts, thereby reducing the equilibrium FA concentration and the corresponding AAR that can be sustained at a given pressure.

From a process design perspective, the lower AAR values obtained at 100 and 120 °C (≈0.75 and ≈0.57, respectively) would require higher steam consumption and increased amine circulation to achieve the same FA production rate. However, when considering the overall time–concentration profiles, the approach to equilibrium at 60 °C was markedly slow, resulting in a low average productivity over a given operating period and, in continuous operation, necessitating longer residence times and larger reactor volumes. In contrast, operation at 80 °C maintained a high equilibrium AAR while providing a more practical balance in terms of productivity. Accordingly, 80 °C was selected as the benchmark operating temperature for the NBIM-based single-amine system, offering the most favorable compromise between AAR and productivity.

To evaluate catalyst stability under the optimized conditions, a recyclability test was conducted (Fig. 3b). After each run, the catalyst

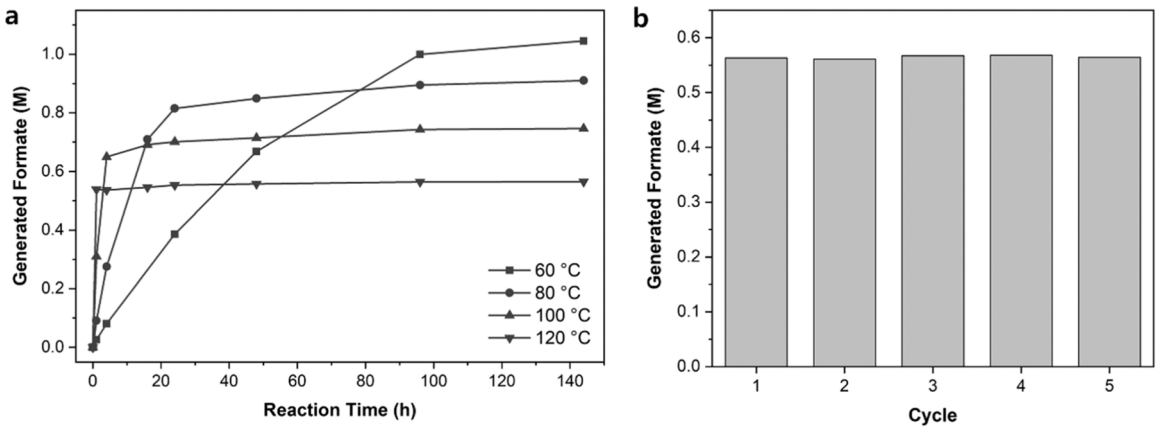


Fig. 3. (a) Time profiles of generated formate at 60, 80, 100, and 120 °C (1–144 h). (b) Recyclability over five consecutive cycles at 80 °C (10 h per cycle).

was readily recovered by simple filtration and reused without additional treatment. The catalytic activity and productivity were well maintained over five consecutive cycles, indicating that the catalyst is stable as a heterogeneous system under the 1.0 M NBIM, 80 °C conditions. In addition, BET analysis after the fifth cycle showed negligible changes in porosity (Fig. S4). To examine possible CO formation from formic acid/formate decomposition, the post-reaction gas phase was analyzed by GC at different reaction temperatures. No detectable CO signal was observed at 80 °C, whereas CO was detected at higher temperatures (Fig. S5) [45].

Under the optimized conditions, the post-reaction solution obtained after cycle 1 was analyzed by ^{1} ^{3}C NMR to examine solution-phase carbon speciation (Fig. S6). ^{1} ^{3}C NMR is widely used in amine-based CO_2 capture/conversion systems to differentiate dissolved CO_2-derived species in solution [48]. Formate and bicarbonate were observed simultaneously, indicating that a fraction of CO_2 remains stabilized in solution as bicarbonate while the remainder is converted to the target product, formate. Such bicarbonate/formate speciation information also supports the need for a degassing/stripping-based regeneration step to remove residual inorganic carbon and restore the base capacity of the amine solution.

Based on the optimized reaction conditions for the single-amine system and the results of catalyst stability tests, we carried out process simulation and an economic assessment.

2.3. TEA-LCA analysis of designed process and prospectives

To evaluate commercial viability, a comprehensive techno-economic analysis (TEA) was conducted using Aspen Plus v14.1 with thermodynamic models validated against experimental data(Fig. S7) [49]. The process comprises reaction and separation sections (Fig. 4a). CO_2 hydrogenation proceeds at 80 bar and 80 °C over Ru-MACHO-POMP in 1 M aqueous NBIM, with reactor sizing extrapolated from batch-derived turnover frequencies [28,37].

Unreacted gases are recovered and recycled to maximize feedstock utilization, while the $NBIMH^{+}{\cdot}HCOO^{-}$ solution is purified through vacuum distillation stages–water separation (D-200), and final purification (D-300)–operated at reduced temperature to prevent formic acid decomposition [8,50,51].

Techno-economic analysis estimates a levelized cost of \$0.583 kg^{-1} for 85 wt% formic acid (Fig. 4e), which falls within the range of reported market prices in North America (\$0.82 kg^{-1}) and India (\$0.89 kg^{-1}). Notably, this CO_2-derived process achieves production costs comparable to or lower than conventional fossil-based routes.

The annualized cost analysis showed that OPEX accounted for 88% of the total cost, whereas CAPEX accounted for the remaining 12%. The Water Separation Column represents the single largest equipment cost (65.3%), as the large water throughput necessitates oversized condenser and reboiler units to handle the associated heat loads (Fig. 4b–d). Cash flow projections indicate a payback period of approximately 6 years based on North American pricing, with potential improvement through carbon credits (Fig. 4f).

However, the life-cycle assessment revealed that the process exhibits a 49% higher global warming potential than conventional routes (Fig. 4g), primarily because of steam consumption in the water-separation step. This finding identifies separation-energy reduction and high-concentration amine operation as the decisive levers for achieving truly low-carbon CCU formic acid production.

We propose a single-amine CO_2 hydrogenation–to–formic acid process using NBIM as the sole amine and demonstrate that, when coupled with a Ru-MACHO-POMP heterogeneous catalyst, meaningful equilibrium AAR and practical productivity can be achieved in 1.0 M aqueous NBIM at a relatively low temperature of 80 °C. Batch experiments show that Ru-MACHO-POMP delivers the highest mass-based productivity among the heterogeneous catalysts evaluated, and approaches AAR $\approx$ 0.9 during extended operation, indicating that NBIM—previously employed solely as a separation amine in dual-amine systems—can simultaneously fulfill both reactive capture and separation functions in a single-amine configuration. Techno-economic analysis further confirms the viability of the proposed process, yielding a competitive levelized cost of formic acid of \$0.583 kg^{-1} , comparable to conventional fossil-based production routes.

However, life-cycle assessment indicates that environmental performance under the current operating conditions (80 °C, 1.0 M NBIM) is constrained by two intrinsic limitations. First, although Ru-MACHO-POMP exhibits superior low-temperature activity compared with conventional heterogeneous catalysts, the space–time yield at 80 °C remains lower than that of dual-amine processes operated at higher temperatures (~120 °C), requiring larger reactor volumes and higher catalyst inventories to achieve comparable FA throughput. This underscores the need for catalyst and process optimization to enhance low-temperature turnover frequencies while retaining the simplicity of the single-amine configuration. Second, operation at a low NBIM concentration (1.0 M) leads to an increased separation energy demand, which offsets the benefit of eliminating the amine-exchange step inherent to dual-amine systems. As a result, TEA and LCA consistently identify steam use in the stripping and distillation sections as the dominant contributor to production cost and greenhouse-gas emissions.

Fig. 5 translates the integrated TEA–LCA outcomes into a quantitative optimization roadmap for the NBIM single-amine platform. The contour maps (Fig. 5a,b) demonstrate that two coupled variables—NBIM aqueous solubility and CO_2-to-formic acid conversion—jointly govern process productivity and the downstream water-removal duty that dominates both cost and environmental

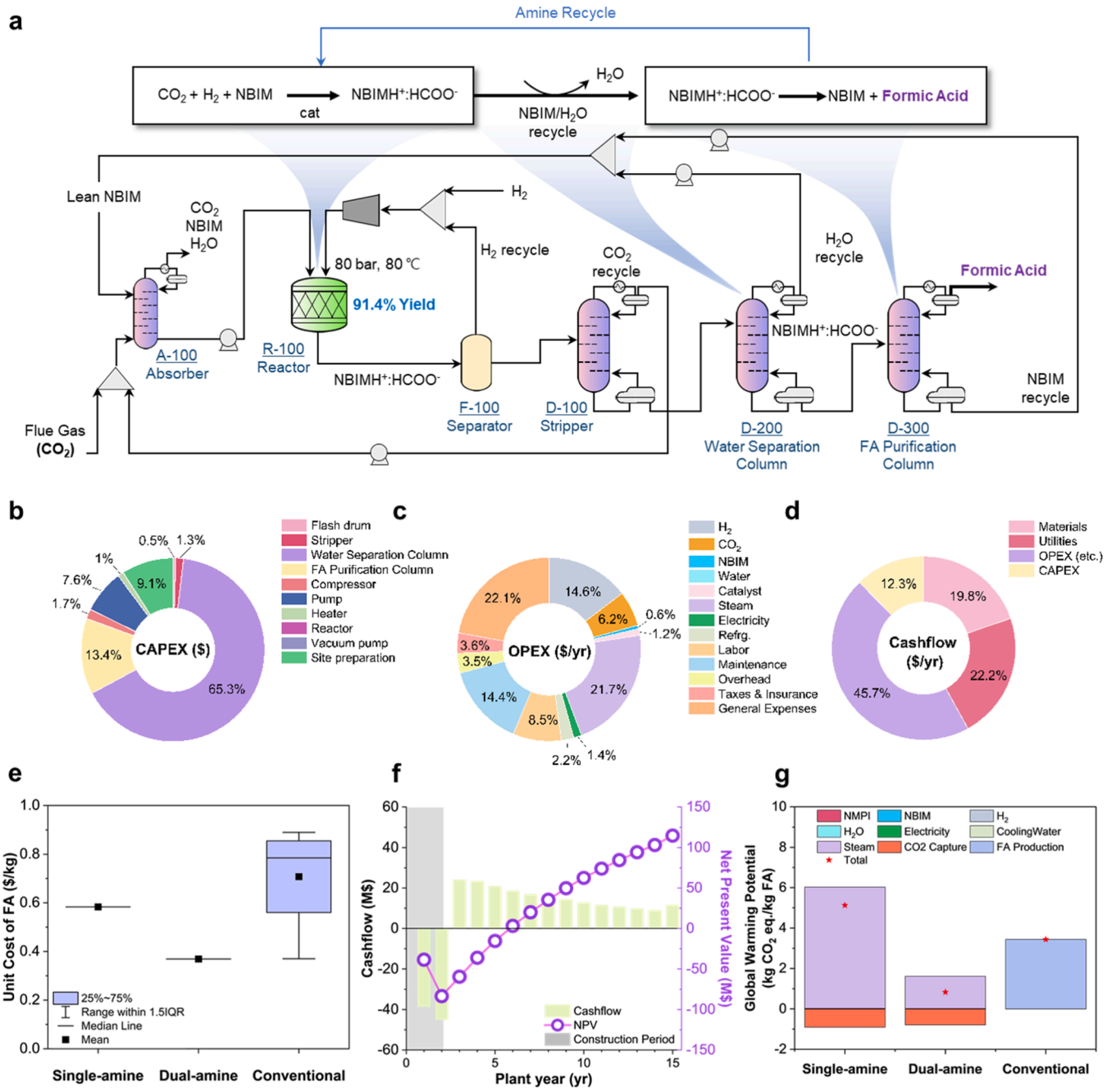


Fig. 4. Techno-economic analysis (TEA) of the proposed single-amine process. a) Schematic of the proposed process. Formic acid stream is indicated with bold line. b-d) Results of the cost breakdown of the overall system. e) Levelized cost of FA comparison between single-amine, dual-amine and conventional FA production. f) Cashflow and net present value representing the overall profitability of the process. g) Comparative global warming potential analysis between three Formic acid production processes.

impact. At the current operating point (red stars), the process has already reached economic competitiveness (LCO < \$0.82 kg^{-1} FA); however, the global warming potential (GWP) remains above the break-even threshold, indicating that the residual performance gap is environmental rather than economic.

Global sensitivity analysis (Fig. 5c) identifies low-pressure steam cost as the dominant contributor to Net Present Value, confirming that separation energy sets the practical boundary of the current design. To further resolve which separation parameters most strongly control environmental performance, we analyzed a combined dataset comprising ±5% perturbations around the baseline and improved designs generated via multi-objective optimization. SHAP analysis (Fig. 5d) reveals that the reboiler duties of columns D200 and D300 are the top two contributors to GWP, far exceeding the influence of other decision variables. This finding provides a mechanistic explanation for the observed behavior: water content in the circulating solvent and the energy required to evaporate it dominate both economic and environmental outcomes.

Based on these insights, process intensification strategies must directly target reboiler heat demand. Mechanical vapor recompression (MVR) was therefore implemented to recover and reutilize latent heat from water vapor, reducing external steam consumption by 50–70%. As shown in Fig. S11, this modification reduces cradle-to-gate GWP from 4.87 to 0.63 kg CO_2-eq kg^{-1} FA while maintaining comparable

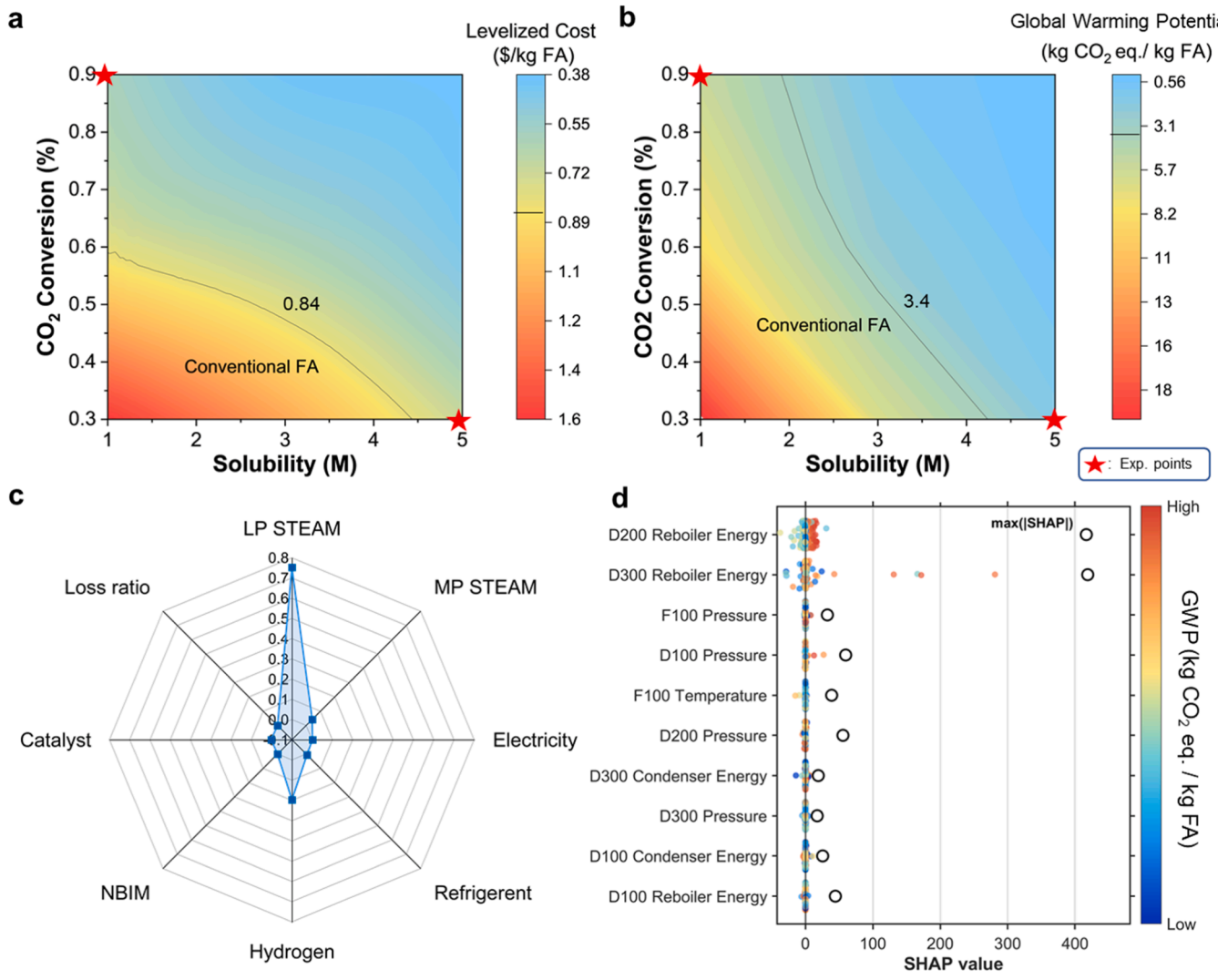


Fig. 5. Sensitivity analysis and optimization roadmap for process parameters. a-b) Contour plots showing the impact of amine solubility and CO_2 conversion on a levelized cost of FA (LCO, $/kg FA) and global warming potential (kg CO_2 eq./kg FA). c) Global sensitivity analysis of eight key cost parameters. d) Strategic optimization framework of process parameters.

equipment costs. Combined with the Pareto front analysis (Fig. S12), which confirms the existence of operating points that minimize LCO and GWP, these results establish high-concentration NBIM operation coupled with separation energy minimization as the decisive route toward an environmentally competitive single-amine RCC process.

3. Conclusions

As a strategy to lower the production cost of formic acid (FA) for liquid organic hydrogen carrier (LOHC) applications, we evaluated the techno-economic feasibility of a new single-amine process that replaces the conventional dual-amine system. Experimentally, Ru-MACHO-POMP delivered the highest productivity among the heterogeneous catalysts tested in a 1.0 M aqueous NBIM system, and the time–concentration profiles confirmed that an AAR of ~0.9 is attainable at 80 °C under this NBIM/H_2O condition. Recycle tests further demonstrated stable catalytic operation under the benchmark conditions. Based on these experimental benchmarks, a techno-economic analysis (TEA) estimated a production cost of \$0.583 kg^{-1} for 85 wt% FA, indicating improved cost competitiveness relative to conventional fossil-resource-based routes. Nevertheless, the analysis also revealed that further system-level improvements are required to enhance economic viability, particularly by maintaining high AAR values under higher amine molarities to reduce downstream separation loads and associated utility demands. With further optimization, the NBIM single-amine process is expected to deliver improved economic viability and environmental sustainability, with the potential to complement or replace conventional fossil-resource-based formic acid production.

4. Methods

4.1. Experimental section

All reagents were purchased from commercial suppliers and used as received without further purification. Ru-MACHO, N-Butylimidazole, Ru/C were purchased from Sigma-Aldrich. Methylene chloride (MC), ethanol and HCl (35–37%) were obtained from Daejung Chemicals. Anhydrous $AlCl_3$ (99.999% purity) was purchased from Alfa Aesar. Deuterated water (D_2O, 99.9%) for NMR analysis was obtained from Cambridge Isotope Laboratories. All the distilled water used in the experiments was obtained via single distillation. High-purity H_2 (99.999%) and CO_2 (99.999%) were supplied by Hanmigas Tech.

4.2. Synthesis of heterogeneous catalysts

Ru-MACHO-POMP. Ru-MACHO-POMP was prepared via

Friedel–Crafts–type hypercross-linking of the Ru-MACHO complex [37]. Ru-MACHO (5.00 g, 8.24 mmol), anhydrous $AlCl_3$ (32 equiv.; 35.14 g, 253.5 mmol), and dry methylene chloride (MC, 250 mL) were charged into an Ace round-bottom pressure flask inside an Ar-filled glovebox. The suspension was heated at 80 °C for 72 h under stirring. After cooling to room temperature, the reaction mixture was carefully quenched with 2 N HCl (50 mL) and stirred for an additional 2 h. The resulting solid was collected by filtration and thoroughly washed with 2 N HCl (500 mL), ethanol (500 mL), and dimethyl carbonate (DMC, 500 mL) until the filtrate became colorless. The solid was then Soxhlet-extracted with ethanol for 48 h and dried under vacuum at 80 °C overnight to afford Ru-MACHO-POMP as a dark brown powder.

$RuCl_3$@$TN_{20}Bpy_1$-CTF and $RuCl_3$@PP-POP. The $RuCl_3$@$TN_{20}Bpy_1$-CTF and $RuCl_3$@DPPE-POP catalysts were synthesized according to our previously reported procedures and used without further modification [28]. Briefly, $TN_{20}Bpy_1$-CTF and PP-POP supports were first prepared as described in the literature, followed by immobilization of $RuCl_3$ onto the porous organic frameworks to give the corresponding Ru-loaded heterogeneous catalysts. The structural and textural properties of $TN_{20}Bpy_1$-CTF, DPPE-POP, and the corresponding Ru-loaded catalysts are described in detail in our previous reports.

4.3. Catalyst characterization

The structural and compositional features of Ru-MACHO-POMP were characterized by FE-SEM, EDS, PXRD, BET, ICP-OES, XPS and NMR.

FE-SEM (Carl Zeiss SIGMA 360) was used to observe surface morphology, and EDS with a 40 mm^2 silicon drift detector provided elemental mapping with a resolution of $\leq$ 127 eV at Mn Kα. PXRD was performed using a Rigaku MiniFlex 300/600 diffractometer (Cu Kα, 40 kV, 15 mA) in 1D scan mode over a 2θ range of 3–90° with a step size of 0.01° at 3.00° min^{-1} . N_2 sorption analysis was carried out at 77 K using a BELSORP-maxII (MicrotracBEL) after degassing at 80 °C for 24 h. Surface area was calculated via the BET method, and pore characteristics were evaluated by BJH analysis. ICP-OES (Agilent 720, KARA) quantified the Ru content to be 10.4 wt%. Measurements were performed with an axial-view torch and simultaneous polychromator (167–782 nm). XPS analysis was performed using a Thermo K-Alpha+ spectrometer with an Al Kα source and hemispherical analyzer to determine surface elemental states. Liquid-state ^{13}C NMR spectra were acquired on a Bruker AVANCE III 400 spectrometer (100 MHz) in D_2O. Spectra were collected without external referencing, using 10,000 scans and a 1.5 s relaxation delay, and were used to qualitatively assess the presence of bicarbonate species. ^{13}C cross-polarization magic-angle spinning solid-state nuclear magnetic resonance spectroscopy (CP MAS NMR) data were analyzed at ambient temperature on a 100.66 MHz Solid-state NMR spectrometer (AVANCE III HD, Bruker, Germany) at the KBSI Western Seoul center with an external magnetic field of 9.4 T (HX CPMAS probe, with 4 mm o.d. Zirconia rotor). Gas chromatography (GC) analyses were performed using a YL-6500 system (Younglin, Korea) equipped with flame ionization and thermal conductivity detectors. Nitrogen was used as the carrier gas at a flow rate of 10 mL/min, and the detection limit for gaseous components was greater than 1 ppm (> 0.0001%).

4.4. Catalytic test

CO_2 hydrogenation was performed in a custom-fabricated 100 mL stainless-steel batch reactor (Fig. S1). Unless otherwise noted, the catalyst, deionized water (17.41 mL), and NBIM (2.48 g, 2.59 mL; 1.0 M in the liquid phase) were added to the reactor. After sealing, the reactor was purged with CO_2 (30 s), followed by CO_2 sparging for 20 min at 300 rpm and pressurization to 40 bar CO_2. The headspace was then pressurized with H_2 to a total pressure of 80 bar (H_2/CO_2 = 1:1). The reactor was heated to the target temperature under stirring (600 rpm) and maintained for the specified reaction time. After reaction, the reactor was cooled to 30 °C, depressurized gradually, and the liquid phase was sampled for HPLC quantification of formic acid.

Time-dependent experiments for kinetic analysis and AAR determination were conducted using the same procedure described above, except that Ru-MACHO-POMP (50 mg) was used and reactions were carried out at 60–120 °C for 1–144 h. After each run, an aliquot of the liquid phase (ca. 0.5–1.0 mL) was withdrawn for HPLC analysis.

When catalyst reuse was evaluated, the solid catalyst (50 mg) was recovered by syringe filtration. For the next run, the catalyst retained on the filter was re-dispersed in 1.0 M NBIM (used as the reaction solvent) and transferred back into the reactor.

Quantitative analysis of formic acid was performed using a Waters Arc HPLC system equipped with a refractive index detector (RID) and an Aminex HPX-87H column. The column temperature was maintained at 50 °C, and 5.00 mM H_2SO_4 was used as the mobile phase at a flow rate of 0.6 mL min^{-1} . Formic acid concentration was determined by external calibration using a seven-point calibration curve ranging from 0.100 to 5.00 M (R^2 = 0.999).

4.5. Process design and simulation

The proposed single-amine process, along with the benchmark dual-amine process and conventional formic acid production process, were rigorously modeled using Aspen Plus v14.1 (Aspentech). The Non-Random Two-Liquid (NRTL) activity coefficient model was selected as the thermodynamic framework to accurately represent the highly non-ideal liquid-phase behavior in amine-containing aqueous systems [52]. The NRTL model is particularly well-suited for capturing the strong hydrogen bonding interactions and electrolyte effects present in amine–formic acid–water mixtures, which are critical for precise prediction of vapor-liquid equilibrium (VLE) in CO_2 capture and conversion processes [53].

The single-amine process flowsheet comprises four main sections: CO_2 thermocatalytic hydrogenation, gas-liquid separation, and product purification, designed for a production capacity of 100,000 metric tons CO_2/year as feedstock. The CO_2-rich NBIM solution is then mixed with makeup NBIM, H_2O, and H_2 before entering a trickle-bed reactor (R-100) operating at 80 bar and 80°C. Based on experimental results, the reactor achieves 91.4% CO_2 conversion with 1.0 M NBIM aqueous solution, producing $NBIMH^+ \cdot HCOO^-$ adduct along with unreacted gases. The reactor effluent is cooled and sent to a flash separator (F-100) where unreacted H_2 and CO_2 are recycled back to the reactor inlet, while the liquid stream proceeds to a stripper column (D-100) under mild vacuum to remove residual dissolved gases.

The core separation challenge lies in selectively recovering high-purity formic acid while recycling NBIM and water through a two-column distillation sequence. The water separation column (D-200) operates at 0.7 bar vacuum with 30 stages, leveraging the preferential bonding between NBIM and FA to distill high-purity water (99.9%) overhead while concentrating the NBIM–FA adduct in the bottom stream. The FA purification column (D-300) operates at 0.35 bar vacuum with 10 theoretical stages to thermally dissociate the NBIM–FA adduct, recovering formic acid as high-purity product (85 wt% or 99 wt %) while recycling NBIM-rich bottoms to the absorber.

4.6. Techno-economic analysis (TEA)

The economic viability of the proposed single-amine-based CO_2 hydrogenation process was assessed through techno-economic analysis (TEA), focusing on key performance indicators including the Levelized Cost of formic acid (LCO), Net Present Value (NPV), and cumulative cash flow. The LCO is defined as the minimum selling price of formic acid at which the project achieves economic break-even (NPV = 0), while the NPV quantifies overall profitability by aggregating discounted cash flows throughout the project lifetime. The fundamental equations

employed for NPV determination are expressed as:

$$NE = (1.0 - t_{income}) \times (S - C_{Excl.Dep.} - D) \quad \text{(TEA-1)}$$

$$CF = (NE + D) - C_{TPI} \quad \text{(TEA-2)}$$

$$NPV = \sum_{n=1}^{N_{life}} \frac{CF_n}{(1+i)^n} \quad \text{(TEA-3)}$$

where NE denotes net earnings, t_{income} represents the corporate income tax rate, S is revenue from product sales, $C_{Excl.Dep}$. indicates production costs excluding depreciation, D is depreciation expense, CF is annual cash flow, C_{TPI} is total permanent investment, and N_{life} is the project duration in years. Economic parameters for NPV calculations were obtained from Seider et al [49]. based on a US plant operation scenario with 2024 as the base year. Operational assumptions for TEA are detailed in Table S2.

$$C_{BM} = C_P \left(\frac{CEPCI_{2024}}{CEPCI_{ref}} \right) F_d F_p F_m F_{BM} \quad \text{(TEA-4)}$$

C_p is the purchased-equipment cost evaluated in the reference year of the adopted sizing–cost correlations, $CEPCI_i$ is the Chemical Engineering Plant Cost Index in year i and F_d, F_p, and F_m are the design, pressure, and material factors, respectively, which account for additional costs under demanding operating conditions (e.g., high-pressure and vacuum operation). F_{BM} is the bare-module factor used to reflect equipment-specific installation and indirect costs. Equipment selection and sizing were determined based on the required processing capacities. Allocation costs were estimated using empirical correlations derived from plant data [49,54,55].

Operating expenditures (OPEX) were estimated using the minimum commercially available prices for materials, catalysts, and utilities, as summarized in Table S4 ~ Table S7. Annual cash flows and NPV were evaluated assuming a 15-year operating lifetime with a 2-year construction period (Table S3). The discount rate was set to twice the nominal U.S. interest rate, and depreciation was calculated using the Modified Accelerated Cost Recovery System (MACRS) with a 7-year recovery period. Both CAPEX and OPEX were evaluated under a base-case assumption that formic acid is sold at U.S. market prices. The TEA results for the single-amine process and the MVR-integrated case are provided in Fig. S13 – Fig. S15, and the global sensitivity ranking is shown in Fig. S16.

To quantify the impact of utility-price fluctuations and other economic uncertainties on process profitability, a global sensitivity analysis (GSA) was conducted by simultaneously varying multiple cost parameters (e.g., raw material prices and loss ratios). GSA captures the combined effects of multiple parameters and is particularly informative when correlations among variables are non-negligible. Variance-based GSA was reported using the first-order sensitivity index:

$$S_i = \frac{\mathrm{var}[E(y|x_i)]}{\mathrm{var}(y)} \quad \text{(TEA-5)}$$

where S_i is the first-order sensitivity index for input i, y is the output metric (NPV in this study), and xi is the uncertain input parameter (e.g., amine unit cost or steam price). The parameters and their variation ranges are summarized in Table S8. Given the dimensionality and computational burden, the Fourier Amplitude Sensitivity Test (FAST) method was employed to efficiently estimate first-order sensitivity indices.

4.7. Life cycle assessment (LCA)

A cradle-to-gate life cycle assessment was conducted to quantify the environmental burdens associated with formic acid production up to the factory gate, in accordance with ISO 14040[56] and ISO 14044[57] frameworks. The system boundaries are illustrated in Fig. S8 and Fig. S9. Environmental impact categories evaluated include global warming potential (GWP), fossil resource scarcity (FRS), and water consumption, using life cycle inventory (LCI) datasets from the Ecoinvent v3.10 database[3 1] and ReCiPe 2016 v1.1 Midpoint (H) method [58,59].

The reported GWP is calculated on a net basis as the difference between process - related CO_2 emissions and CO_2 uptake. For the baseline case, the LCI entry exhibiting the CO_2 emission factor among available supplier/geography-specific datasets was adopted, while the full range of reported LCI variability was propagated in the sensitivity analysis using the statistics summarized in Table S9. Benchmark LCI data representing conventional industrial formic acid production routes were compiled separately (Table S10).

Because an LCI dataset for NMPI was not available, N-methyl-2-pyrrolidone (NMPO), a structurally similar solvent, was used as a surrogate. Blue hydrogen produced via steam methane reforming (SMR) with carbon capture and storage (CCS) was assumed as the baseline H_2 source. Vent streams were modeled as being fully oxidized in a recuperative thermal oxidizer, and the resulting CO_2 emissions were included in the inventory. Overall LCA results are reported in Fig. 4g, with supporting LCI statistics and benchmark inventories provided in Table S9–S10 and system boundary schematics in Figs. S8–S9.

4.8. Multi-objective optimization and analysis of key process variables

Multi-objective optimization was performed by coupling an NSGA-II genetic algorithm with Aspen Plus as an in-the-loop process simulator. Two objectives were minimized simultaneously: levelized cost of formic acid (LCO, \$ kg^{-1} FA) and cradle-to-gate global warming potential (GWP, kg CO_2-eq kg^{-1} FA). The decision space comprised 11 separation-train operating variables: flash drum temperature and pressure (F100), and distillation specifications for three columns (D100–D300) including condenser/reboiler duties, distillate-to-feed ratios, and operating pressures. Each variable was bounded within approximately ±5% of the base case to maintain robust convergence in the tightly heat- and mass-integrated flowsheet. Economic and environmental indicators were computed consistently through integrated TEA/LCA routines, accounting for electricity, steam, cooling duties, and net CO_2 balance.

To reduce expensive Aspen calls, a gradient-boosted decision tree (GBDT) surrogate ensemble was trained to approximate LCO, GWP, and FA purity as functions of the 11 decision variables. Sample weights were assigned based on FA purity (≥85 wt%) to focus learning near the feasibility boundary. The NSGA-II search was executed primarily on the surrogate, with candidates violating the FA ≥ 85 wt% constraint penalized accordingly. A diversity-aware selection rule chose candidates per iteration for parallel Aspen validation; validated solutions that remained non-dominated were stored in the Pareto archive, and surrogate models were retrained as the dataset expanded.

Key process drivers were identified using SHAP (SHapley Additive exPlanations) analysis on the trained surrogate models. SHAP values for LCO and GWP were computed on the combined dataset (initial sampling + validated optimization results) by estimating each feature's marginal contribution to the prediction. Beeswarm plots were generated to visualize the magnitude and directionality of each variable's impact, with feature values mapped to color via min–max normalization to distinguish high versus low operating conditions.

CRediT authorship contribution statement

Minsol Kim: Writing – review & editing, Software, Methodology, Investigation. **Sungho Yoon:** Writing – review & editing, Supervision, Project administration, Funding acquisition. **Jiseong Baek:** Writing – review & editing, Writing – original draft, Visualization, Validation, Supervision, Software, Resources, Project administration, Methodology, Investigation, Formal analysis, Data curation, Conceptualization. **Jaehyeong Choi:** Writing – review & editing, Writing – original draft,

Visualization, Validation, Software, Resources, Methodology, Investigation, Formal analysis, Data curation. **Hongjin Park:** Writing – review & editing, Project administration, Investigation, Data curation, Conceptualization. **Ki Bong Lee:** Funding acquisition, Project administration, Writing – review & editing. **Ung Lee:** Writing – review & editing, Supervision, Project administration, Funding acquisition.

Declaration of Competing Interest

The authors declare that they have no known competing financial interests or personal relationships that could have appeared to influence the work reported in this paper.

Acknowledgements

This work was supported by National Research Foundation of Korea (NRF-2022M3C1A3092056) and the Global Science Research Center Program (RS-2024-00411134) funded by the National Research Foundation of Korea, and the Chung-Ang University Graduate Research Scholarship in 2025.

Appendix A. Supporting information

Supplementary data associated with this article can be found in the online version at doi:10.1016/j.jcou.2026.103426.

Data availability

Data will be made available on request.

References

[1] J. Artz, T.E. Müller, K. Thenert, J. Kleinekorte, R. Meys, A. Sternberg, A. Bardow, W. Leitner, Sustainable conversion of carbon dioxide: an integrated review of catalysis and life cycle assessment, Chem. Rev. 118 (2018) 434–504, https://doi.org/10.1021/acs.chemrev.7b00435.
[2] G.A. Olah, Beyond oil and gas: the methanol economy, Angew. Chem. - Int. Ed. 44 (2005) 2636–2639, https://doi.org/10.1002/anie.200462121.
[3] A. Otto, T. Grube, S. Schiebahn, D. Stolten, Closing the loop: captured CO2 as a feedstock in the chemical industry, Energy Environ. Sci. 8 (2015) 3283–3297, https://doi.org/10.1039/c5ee02591e.
[4] C. Ampelli, S. Perathoner, G. Centi, Co2 utilization: an enabling element to move to a resource-and energy-efficient chemical and fuel production, Philos. Trans. R. Soc. A Math. Phys. Eng. Sci. 373 (2015), https://doi.org/10.1098/rsta.2014.0177.
[5] R. Ye, J. Ding, W. Gong, M.D. Argyle, Q. Zhong, Y. Wang, C.K. Russell, Z. Xu, A. G. Russell, Q. Li, M. Fan, Y. Yao, CO2 hydrogenation to high-value products via heterogeneous catalysis, Nat. Commun. (2019), https://doi.org/10.1038/s41467-019-13638-9.
[6] M. Yousaf, M. Zaman, A. Mahmood, A. Elkamel, M. Rizwan, M. Imran, T. Wilberforce, Carbon dioxide utilization: a critical review from multiscale perspective. 2022. pp. 4890–4923. https://doi.org/10.1002/ese3.1303..
[7] D. Wei, S. Rui, P. Sponholz, Henrik Junge, M. Beller, Reversible hydrogenation of carbon dioxide to formic acid using a Mn-pincer complex in the presence of lysine, Nat. Energy 7 (2022) 438–447, https://doi.org/10.1038/s41560-022-01019-4%0AReversible.
[8] D. Mellmann, P. Sponholz, H. Junge, M. Beller, Formic acid as a hydrogen storage material-development of homogeneous catalysts for selective hydrogen release, Chem. Soc. Rev. 45 (2016) 3954–3988, https://doi.org/10.1039/c5cs00618j.
[9] F. Meng, Z. Shen, X. Lin, P. Song, T. Wu, S. Xi, C. Wu, Z. Ma, D. Mandler, Z.J. Xu, Industrially viable formate production with 50% lower CO2 emissions, Energy Environ. Sci. 18 (2025) 3680–3688, https://doi.org/10.1039/d5ee00452g.
[10] S.C. Huang, C.C. Cheng, Y.H. Lai, C.Y. Lin, Sustainable and selective formic acid production from photoelectrochemical methanol reforming at near-neutral pH using nanoporous nickel-iron oxyhydroxide-borate as the electrocatalyst, Chem. Eng. J. 395 (2020) 125176, https://doi.org/10.1016/j.cej.2020.125176.
[11] K. Park, H. Park, H. Yoon, K.R. Lee, S. Ahn, C. Kim, U. Lee, K.D. Jung, S. Yoon, Recent progress in heterogeneous CO2 hydrogenation to formic acid towards practical application, Catal. Sci. Technol. 14 (2024) 5811–5832, https://doi.org/10.1039/d4cy00798k.
[12] G.H. Gunasekar, K. Park, K.D. Jung, S. Yoon, Recent developments in the catalytic hydrogenation of CO2 to formic acid/formate using heterogeneous catalysts, Inorg. Chem. Front 3 (2016) 882–895, https://doi.org/10.1039/c5qi00231a.
[13] K. Sordakis, C. Tang, L.K. Vogt, H. Junge, P.J. Dyson, M. Beller, Homogeneous catalysis for sustainable hydrogen storage in formic acid and alcohols.2018, https://doi.org/10.1021/acs.chemrev.7b00182..
[14] D.A. Bulushev, J.R.H. Ross, Heterogeneous catalysts for hydrogenation of CO 2 and bicarbonates to formic acid and formates, Catal. Rev. 60 (2018) 566–593, https://doi.org/10.1080/01614940.2018.1476806.
[15] G.A. Cuevas-Castillo, S. Michailos, K. Hughes, D. Ingham, F. Navarro-Pineda, M. Pourkashanian, Techno-economic and life cycle assessment of power-to-formic acid production using direct air capture and green hydrogen, Clean. Eng. Technol. 26 (2025) 100929, https://doi.org/10.1016/j.clet.2025.100929.
[16] C.J. Gerack, L. McElwee-White, Formylation of amines, Molecules 19 (2014) 7689–7713, https://doi.org/10.3390/molecules19067689.
[17] S. Laporte, F. Pietrucci, F. Guyot, A.M. Saitta, Formic acid synthesis in a water-mineral system: major role of the interface, J. Phys. Chem. C. 124 (2020) 5125–5131, https://doi.org/10.1021/acs.jpcc.9b09979.
[18] A. Álvarez, A. Bansode, A. Urakawa, A.V. Bavykina, T.A. Wezendonk, M. Makkee, J. Gascon, F. Kapteijn, Challenges in the greener production of formates/formic acid, methanol, and dme by heterogeneously catalyzed CO2 hydrogenation processes, Chem. Rev. 117 (2017) 9804–9838, https://doi.org/10.1021/acs.chemrev.6b00816.
[19] N. Kusuo, S. MinoruVapor-liquid equilibrium for formic acid-triethylamine system examined by the use of modified Still. Formic Acid-Trialkylamine Azeotopes, 1977. pp. 135–140.
[20] A.W.N. de Leeuw den Bouter, L.M.P. Meijer, L. Brito, A. Miquelot, P. Olivier, J. van der Schaaf, Effect of tertiary amine selection on CO_2 to formic acid hydrogenation with the Au-np catalyst, Ind. Eng. Chem. Res. 64 (2025) 8109–8118, https://doi.org/10.1021/acs.iecr.4c04902.
[21] C. M. De Brito Mendes, J. Rubio, F. Rebelo, S. Santos, J. Öner, V.V. Ordomsky, M. Saeys, Role of base in CO2 hydrogenation to formate over a Ru(III) solid micellar catalyst, Catal. Sci. Technol. 15 (2025) 5327–5334, https://doi.org/10.1039/d5cy00662g.
[22] A.W.N. de Leeuw den Bouter, E.J.M. Vogels, A. Miquelot, L. Brito, P. Olivier, J. van der Schaaf, Chemical and phase equilibrium of formic acid-trialkylamine complexes, ACS Omega 10 (2025) 27735–27744, https://doi.org/10.1021/acsomega.4c10897.
[23] E. Barbera, F. Mantoan, A. Bertucco, F. Bezzo, Hydrogenation to convert CO 2 to C1 chemicals: Technical comparison of different alternatives by process simulation, (2020) 1893–1906. https://doi.org/10.1002/cjce.23755.
[24] B. Mahida, H. Benyounes, S. Jin, W. Shen, Pressure-swing distillation process for separating ternary azeotropic mixture of acidic aqueous solution, Chem. Eng. Commun. 209 (2022) 882–894, https://doi.org/10.1080/00986445.2021.1925653.
[25] G. Ren, Continuous production of pure formic acid solution from CO 2 hydrogenation at room temperature via amine-functionalized PdMn, Chem. Eng. J. 497 (2024) 154951, https://doi.org/10.1016/j.cej.2024.154951.
[26] T.A. Atsbha, H.J. Yoon, A. Cherif, C.J. Lee, Feasibility and sustainability of emerging CCU pathways for formic acid production, Green. Chem. 26 (2024) 10982–10995, https://doi.org/10.1039/d4gc02507e.
[27] C. Kim, Y. Lee, K. Kim, Implementation of formic acid as a liquid organic hydrogen carrier (LOHC): techno-economic analysis and life cycle assessment of formic acid produced via CO 2 utilization, (2022).
[28] K. Park, G.H. Gunasekar, S.H. Kim, H. Park, S. Kim, K. Park, K.D. Jung, S. Yoon, CO2 hydrogenation to formic acid over heterogenized ruthenium catalysts using a fixed bed reactor with separation units, Green Chem. 22 (2020) 1639–1649, https://doi.org/10.1039/c9gc03685g.
[29] C. Kim, K. Park, H. Lee, J. Im, D. Ususky, K. Tak, D. Park, W. Chung, D. Han, J. Yoon, H. Lee, H. Kim, Margareth, J. Jung, D.H. Won, C.J. Yoo, K.B. Lee, K. D. Jung, U. Lee, Accelerating the net-zero economy with CO2-hydrogenated formic acid production: process development and pilot plant demonstration, Joule 8 (2024) 693–713, https://doi.org/10.1016/j.joule.2024.01.003.
[30] D. Ususky, U. Lee, K.-D. Jung, C. Kim, K. Kim, Optimized distillation design for CCU-based formic acid process: a combined experimental and modeling approach, Chem. Eng. Ind. Chem. (2025). ⟨https://chemrxiv.org/engage/chemrxiv/article-details/68809b1c23be8e43d68f8f89⟩.
[31] J.F. Hull, Y. Himeda, W.H. Wang, B. Hashiguchi, R. Periana, D.J. Szalda, J. T. Muckerman, E. Fujita, Reversible hydrogen storage using CO 2 and a proton-switchable iridium catalyst in aqueous media under mild temperatures and pressures, Nat. Chem. 4 (2012) 383–388, https://doi.org/10.1038/nchem.1295.
[32] K. Rohmann, J. Kothe, M.W. Haenel, U. Englert, M. Hölscher, W. Leitner, Hydrogenation of CO2 to formic acid with a highly active ruthenium acriphos complex in DMSO and DMSO/water, Angew. Chem. - Int. Ed. 55 (2016) 8966–8969, https://doi.org/10.1002/anie.201603878.
[33] A. Boddien, D. Mellmann, F. Gärtner, R. Jackstell, H. Junge, P.J. Dyson, G. Laurenczy, R. Ludwig, M. Beller, Efficient dehydrogenation of formic acid using an iron catalyst, Science 333 (6050) (2011) 1733–1736, https://doi.org/10.1126/science.1206613.
[34] R. Sun, Y. Liao, S.T. Bai, M. Zheng, C. Zhou, T. Zhang, B.F. Sels, Heterogeneous catalysts for CO2 hydrogenation to formic acid/formate: From nanoscale to single atom, Energy Environ. Sci. 14 (2021) 1247–1285, https://doi.org/10.1039/d0ee03575k.
[35] A. Nisters, N. Heim, M. Rose, Influence of phosphine macroligands in solid molecular ruthenium catalysts on the hydrogenation of CO2 to formate, J. Catal. 442 (2025) 115853, https://doi.org/10.1016/j.jcat.2024.115853.
[36] Z. Liu, T. Yang, Y. Song, N. Zhao, S. Wu, Z. Ma, X. Gong, X. Tian, Z. Liu, Hypercrosslinked polymer by an external crosslinker strategy: formation mechanism, structural regulation and applications, RSC Appl. Polym. 3 (2025) 746–766, https://doi.org/10.1039/d4lp00379a.

[37] H. Park, K. Park, U. Lee, S. Yoon, Sustainable formate production via highly active CO2 hydrogenation using porous organometallic polymer with Ru-PNP active sites, ChemSusChem 18 (2025) 6–11, https://doi.org/10.1002/cssc.202402038.
[38] S. Padmanaban, Y. Lee, S. Yoon, Chemoselective hydrogenation of α,β-unsaturated carbonyl compounds using a recyclable Ru catalyst embedded on a bisphosphine based POP, J. Ind. Eng. Chem. 94 (2021) 361–367, https://doi.org/10.1016/j.jiec.2020.11.007.
[39] H. Ghorbani, A. Nezami, B. Sheikholeslami, A. Hedjazi, M. Ahmadimanesh, Simultaneous measurement of formic acid, methanol and ethanol in vitreous and blood samples of postmortem by headspace GC-FID, J. Occup. Med. Toxicol. 13 (2018) 4–11, https://doi.org/10.1186/s12995-017-0184-3.
[40] K. Park, K.R. Lee, S. Ahn, H. Park, S. Moon, S. Yoon, K.-D. Jung, Investigating the catalytic deactivation of a Pd catalyst during the continuous hydrogenation of CO2 into formate using a trickle-bed reactor, Catalysts 14 (2024) 187, https://doi.org/10.3390/catal14030187.
[41] G. Hariyanandam Gunasekar, S. Padmanaban, K. Park, K.-D. Jung, S. Yoon, An efficient and practical system for the synthesis of N,N-dimethylformamide by CO2 hydrogenation using a heterogeneous Ru catalyst:from batch to continuous flow, ChemSusChem 13 (2020) 1735–1739.
[42] J. Paik, J.H. Choe, S. Padmanaban, M. Seo, C.J. Yoo, H.B. Lee, Y. Lee, Thermodynamic hydricity of a ruthenium CO2 hydrogenation catalyst supported by a rigid PNP pincer, JACS Au 5 (2025) 811–821, https://doi.org/10.1021/jacsau.4c01078.
[43] G.A. Filonenko, E.J.M. Hensen, E.A. Pidko, Mechanism of CO2 hydrogenation to formates by homogeneous Ru-PNP pincer catalyst: from a theoretical description to performance optimization, Catal. Sci. Technol. 4 (2014) 3474–3485, https://doi.org/10.1039/c4cy00568f.
[44] G.A. Filonenko, R. Van Putten, E.N. Schulpen, E.J.M. Hensen, E.A. Pidko, Highly efficient reversible hydrogenation of carbon dioxide to formates using a ruthenium PNP-pincer catalyst, ChemCatChem 6 (2014) 1526–1530, https://doi.org/10.1002/cctc.201402119.
[45] H. Park, S. Moon, S. Yoon, CO2 conversion into formic acid with CO-containing hydrogen gas over a heterogenized Ru catalyst, J. CO2 Util. 98 (2025) 103154, https://doi.org/10.1016/j.jcou.2025.103154.
[46] M.D. Morton, B.Y. Tay, J.J.Q. Mah, A.J.P. White, J.D. Nobbs, M. van Meurs, G.J. P. Britovsek, Hydrogen activation with Ru-PN3P pincer complexes for the conversion of C1 feedstocks, Inorg. Chem. 63 (2024) 3393–3401, https://doi.org/10.1021/acs.inorgchem.3c04001.
[47] C. Fink, M. Montandon-Clerc, G. Laurenczy, Hydrogen storage in the carbon dioxide-formic acid cycle, Chimia 69 (2015) 746–752, https://doi.org/10.2533/chimia.2015.746.
[48] C. Perinua, B. Arstad, K.-J. Jens, ^{13}C NMR experiments and methods used to investigate amine-CO2-H2O systems, Energy Procedia 37 (2013) 7310–7317.
[49] W.D. Seider, D.R. Lewin, J.D. Seader, S. Widagdo, R. Gani, K.M. Ng. Product and Process Design Principles: Synthesis, Analysis and Evaluation, 4th ed., John Wiley & Sons, New York, 2016.
[50] J. Yu, P.E. Savage, Decomposition of formic acid under hydrothermal conditions, Ind. Eng. Chem. Res. 37 (1998) 2–10, https://doi.org/10.1021/ie970182e.
[51] W. Marczak, M.A. Varfolomeev, I.T. Rakipov, P. Lodowski, K. Kowalska-Szojda, M. Łężniak, L. Almásy, A. Len, Molecular aggregation in binary mixtures of pyrrolidine, n-methylpyrrolidine, piperidine, and N-methylpiperidine with water: thermodynamic, SANS, and theoretical studies, J. Phys. Chem. B 121 (2017) 3070–3086, https://doi.org/10.1021/acs.jpcb.6b10262.
[52] Aspen Technology Inc, Rate-based model of the CO2 capture process by MEA using Aspen Plus, (2012).
[53] H. Renon, J.M. Prausnitz, Estimation of parameters for the nrtl equation for excess gibbs energies of strongly nonideal liquid mixtures, Ind. Eng. Chem. Process Des. Dev. 8 (1969) 413–419, https://doi.org/10.1021/i260031a019.
[54] J.L. Sorrels, A. Baynham, D. Randall, C. Hancy, U.S. EPA AP-42, Volume I, Chapter 2: Incinerators and Oxidizers, Research Triangle Park, 2017.
[55] L.T. Biegler, I.E. Grossmann, A.W. WesterbergSystematic methods of chemical process design, 1999. 796.
[56] International Organization for Standardization (ISO), ISO 14040: Environmental assessment - Life cycle assessment - Principles and framework, Geneva, 2006.
[57] International Organization for Standardization (ISO), ISO 14044: Environmental management - Life cycle assessment - Requirements and guidelines, Geneva, 2006.
[58] G. Wernet, C. Bauer, B. Steubing, J. Reinhard, E. Moreno-Ruiz, B. Weidema, The ecoinvent database version 3 (part I): overview and methodology, Int. J. Life Cycle Assess. 21 (2016) 1218–1230, https://doi.org/10.1007/s11367-016-1087-8.
[59] M.A.J. Huijbregts, Z.J.N. Steinmann, P.M.F. Elshout, G. Stam, R. Van Zelm, ReCiPe2016: a harmonised life cycle impact assessment method at midpoint and endpoint level, Int. J. Life Cycle Assess. (2017) 138–147, https://doi.org/10.1007/s11367-016-1246-y.